The littoral zone of polar lakes: Inshore-offshore contrasts in an ice-covered High Arctic lake

Paschale N. Bégin[1,2], Milla Rautio[1,3], Yukiko Tanabe[4,5], Masaki Uchida[4,5], Alexander I. Culley[1,6] and Warwick F. Vincent[1,2]

Affiliations

[1]Centre d'études nordiques (CEN) & Takuvik Joint International Laboratory, Quebec City, Quebec, Canada

[2]Département de biologie, Université Laval, Quebec City, Quebec, Canada

[3]Département des sciences fondamentales, Université du Québec à Chicoutimi, Chicoutimi, Quebec, Canada

[4]National Institute of Polar Research, Tachikawa, Japan

[5]The Graduate University for Advanced Studies, SOKENDAI

[6]Département de biochimie, de microbiologie et de bio-informatique, Université Laval, Quebec City, Quebec, Canada

Correspondence

Corresponding authors:

Paschale N. Bégin pnbegin@gmail.com ORCID: 0000-0002-1031-3559

Warwick F. Vincent warwick.vincent@bio.ulaval.ca ORCID: 0000-0001-9055-1938

© The Author(s) or their Institution(s)

Co-authors:

Milla Rautio milla_rautio@uqac.ca ORCID 0000-0002-2375-9082

Yukiko Tanabe ukkopu@gmail.com

Masaki Uchida uchida@nipr.ac.jp

Alexander I. Culley alexander.culley@bcm.ulaval.ca ORCID 0000-0001-6639-9112

For submission to the *Arctic Science* special issue "Terrestrial Geosystems, Ecosystems and Human Systems in the Fast-Changing Arctic".

© The Author(s) or their Institution(s)

Abstract

In ice-covered polar lakes, a narrow ice-free moat opens up in spring or early summer, and then persists at the edge of the lake until complete ice loss or refreezing. In this study, we analyzed the horizontal gradients in Ward Hunt Lake, located in the High Arctic, and addressed the hypothesis that the transition from its nearshore open-water moat to offshore ice-covered waters is marked by discontinuous shifts in limnological properties. Consistent with this hypothesis, we observed an abrupt increase in below-ice concentrations of chlorophyll *a* beyond the ice margin, along with a sharp decrease in temperature and light availability and pronounced changes in benthic algal pigments and fatty acids. There were higher concentrations of rotifers and lower concentrations of viruses at the ice-free sampling sites, and contrasts in zooplankton fatty acid profiles that implied a greater importance of benthic phototrophs in their inshore diet. The observed patterns underscore the structuring role of ice cover in polar lakes. These ecosystems do not conform to the traditional definitions of littoral versus pelagic zones, but instead may have distinct moat, ice-margin and ice-covered zones. This zonation is likely to weaken with ongoing climate change.

Keywords: lake zonation, lake ice, food webs, microbial mats, underwater light

© The Author(s) or their Institution(s)

Introduction

Lakes are sentinels of environmental change and integrate the conditions of their surrounding watersheds (Williamson et al. 2009). The shallow nearshore portion of a lake, the littoral zone, is the interface between water and land, and plays a key role in the whole lake ecosystem and its responses to change (Vander Zanden and Vadeboncoeur 2020). Dissolved and particulate nutrients enter the littoral zone by inflows from the watershed and influence primary production throughout the lake (Jones et al. 1998). In oligotrophic lakes, ecosystem productivity is the result of not only autochthonous processes but also heterotrophic production fuelled by allochthonous organic carbon entering the littoral zone from terrestrial sources (Ask et al. 2009). These inputs of detrital organic matter are a potential food source for zoobenthos (Solomon et al. 2011) and zooplankton (Rautio et al. 2011; Harfmann et al. 2019), and can stimulate bacterial production (Traving et al. 2017). The presence of macrophytes along with associated periphyton supports a productive inshore benthic habitat, especially in oligotrophic lakes (Vadeboncoeur et al. 2008). However, the abundance and composition of the biota in the littoral zone can be seasonally influenced by changing inflow conditions, and by the combined mechanical effects of suspended particles, wave action and ice that alter near-shore sediments and vegetation (Strayer and Findlay 2010), thereby affecting the whole lake ecosystem.

A variety of definitions have been proposed to set the boundary between inshore (littoral) and offshore (pelagic or limnetic) zones of lakes, and these have differed among fields of study such as hydrology, biology and geomorphology. The littoral zone can be broadly defined as the region where land processes and the aquatic ecosystem influence one another (Strayer and Findlay 2010), and more specifically as the area where at least 1% of incoming photosynthetically available radiation (PAR, 400-700 nm) reaches the bottom and allows macrophytes to grow (Peters and

© The Author(s) or their Institution(s)

Lodge 2009). In High Arctic and Antarctic lakes, however, vascular plants are absent, and hardy mosses and microbial biofilms are the only phototrophs colonizing the sediments of inshore waters (Sand-Jensen et al. 1999; Mohit et al. 2017). These shallow waters freeze to the sediments in winter, and the habitats are subject to the additional stress of scouring by ice movements during melt-out. Light availability in polar lakes is constrained more by ice cover and the extreme seasonality of solar variation rather than by the depth of the water column, further underscoring the difficulty of applying a temperate latitude definition of 'littoral zone' to high latitude aquatic ecosystems.

Arctic and Antarctic lakes are commonly covered by a thick ice cover that remains for most or even all of the year and that greatly reduces the annual input of light to the water column (Schindler et al. 1974). In early summer, the ice cover begins to melt at its edge, producing a narrow ice-free band of open water along the shore of the lake. This 'moat' region provides the only area of direct exchange with the atmosphere, allowing wind-induced turbulence, exposure to incident solar radiation and full gas exchange with the overlying air, along with input of water from the surrounding watershed (Priscu et al. 1996; Hall et al. 2017). Few studies, however, have examined these inshore features and processes in detail. The early inshore melting is driven by the higher input of solar energy per unit ice volume in these shallow depths, with positive feedback effects caused by the increasing amounts of resultant meltwater that heat up in the shallows. After the initial rapid melt-out towards deeper water, the central pan of floating ice may then rest in place for a long period of time, sometimes anchored on one side of the lake according to wind direction, and with a potentially strong influence on underwater light and photosynthesis (Belzile et al. 2001).

In the present study, we focused on the inshore-offshore gradients in Ward Hunt Lake in the Canadian High Arctic. This far northern lake is covered by thick ice for at least 11 months of the year, and in many years by multi-year ice that persists throughout summer (Paquette et al. 2015).

© The Author(s) or their Institution(s)

In all years, even in the past when the lake was covered by 4-m thick perennial ice, a moat of open water has extended around more than half the shoreline, persisting for several weeks each summer (Paquette et al. 2015; Bégin et al. 2020). We sampled along transects from the lake-edge moat to sub-ice waters in the middle of the lake to address the hypothesis that there would be an inshore-offshore discontinuity in limnological properties that is directly linked to the ice cover. This study is a contribution to the project 'Terrestrial Multidisciplinary distributed Observatories for the Study of Arctic Connections' (T-MOSAiC), which places emphasis on system-level properties, including connectivity, gradients and discontinuities (Vincent et al. 2019).

Materials and methods

Study site

Ward Hunt Lake (83°05.226'N; 74°08.721'W; WGS84 map datum), is Canada's northernmost lake and is covered by thick annual or multi-year ice. It is located on Ward Hunt Island, 6 km off the northern coast of Ellesmere Island (Nunavut, Canada; Supplementary Fig. S1), and has an area of 0.37 km^2 and a maximum recorded depth of 9.7 m. The region is influenced by a polar desert climate with a mean annual air temperature of -16.7°C and a July average temperature of 1.7°C (2006-2018; CEN 2020). Ward Hunt Lake is mainly fed by meltwater from snow patches in its 1.82 km^2 watershed, which flows into the lake via surface and subsurface water tracks (Paquette et al. 2020). The ice phenology and moat formation in Ward Hunt Lake were observed with time-lapse images captured by an automated camera on its western shore, at hourly intervals from 10:00 to 14:00 h each day. The camera was in function from 25 June to 31 October 2016, from 18 July to 7 November 2017 and from 25 May 2018 to 21 April 2019. The full dataset of

© The Author(s) or their Institution(s)

images and the details about the camera installation are archived in the Nordicana D data repository (NEIGE 2020).

Physicochemical variables

In July 2015, four sites were sampled along three replicate transects that covered the inshore-offshore gradient, extending out from the northwestern shore of the lake (Fig. 1). Samples from the inshore moat site (S1) were collected within 5 m of the shore. Samples from the ice-margin site (S2) were obtained in the open-water area within 2 m of the edge of the ice cover, which was located approximately 20 m from the shore. A sampling of the intermediate under-ice site (S3) was at a distance of about 100 m from the shore and corresponded to under-ice conditions approximately mid-distance between the deepest part of the lake and the shore. Samples at the central under-ice site (S4) were collected beneath the ice at this location of the greatest water column depth. Samples were collected between 14 and 21 July 2015. Oxygen, temperature, pH and conductivity profiles were measured using a DS5X (Hydrolab, Loveland, CO) and a 600QS probe (YSI, Yellow Springs, OH).

Light profiles from 280 to 720 nm were measured in July 2016 with a RAMSES ACC UV/VIS hyperspectral irradiance sensor (TriOS, Germany) from the four sites as shown in Figure 1. The diffuse attenuation coefficient (K_d) was calculated as:

$$K_d = -\ln(E_2/E_1)/(z_2-z_1) \quad (1)$$

where E_1 is the irradiance at the higher depth z_1, and E_2 is the irradiance at the lower depth z_2. Comparisons were made between the surface waters at S1 and few centimetres below the ice (at around 2 m depth relative to the upper ice surface) in the central under-ice site (site S4). Lake

© The Author(s) or their Institution(s)

water was sampled through the ice in the intermediate and central sites with a 7-litre Limnos Water Sampler (Limnos, Poland) and directly at the surface from a boat for the ice margin and inshore moat sites. Microbial mat samples at S1 were collected by wading out from the shore, whereas those at S3 and S4 were collected with a Mini-Glew corer (Glew 1991). Microbial mats were not sampled at S2.

Water for coloured dissolved organic matter (CDOM), dissolved organic carbon (DOC) and dissolved inorganic carbon (DIC) was collected in July 2017 and filtered through pre-rinsed cellulose acetate filters (0.2 μm porosity), then stored without headspace in tightly capped glass bottles at 4°C in the dark until analysis. DOC and DIC concentrations were measured with infrared detection in a total organic carbon analyzer (TOC-VCPH, Shimadzu, Japan) after catalytic combustion. The absorbance of CDOM ($A_{CDOM}(\lambda)$) was measured from 200 to 800 nm at 1 nm intervals with a Varian Cary 100 dual-beam spectrophotometer (Varian Inc., Canada). Following the protocol described by Helms et al. (2008), we conducted a null point correction by subtracting the mean $A_{CDOM}(\lambda)$ from 750 to 800 nm from the complete spectrum after the subtraction of the blank, and the values were converted to CDOM absorption ($a_{CDOM}(\lambda)$).

Water for spectral absorption measurements of suspended particles was collected at the surface in the inshore moat site (S1) and just below the ice in the central site (S4) and filtered through 25 mm GF/F filters that were preserved at -80°C until analysis. The optical density of the material collected on the filters was measured at wavelengths from 300 to 720 nm in a Varian Cary 100 dual-beam spectrophotometer (Agilent, Santa Clara, California) equipped with an integrating sphere (Labsphere Inc., North Sutton, New Hampshire) . Filters were then treated with 65°C pure methanol to remove all pigments and determine non-algal particle absorption (a_{NAP}; Kishino et al., 1985; Mitchell et al., 2002). Total particulate absorption (a_p) was calculated as:

© The Author(s) or their Institution(s)

$$a_p = [2.303 * (OD_{fp} - OD_{null})] / \left[\beta^{\lambda} * \frac{V_f}{A_f}\right] \quad (2)$$

where OD_{fp} is the optical density of the sample between 250 and 750 nm, OD_{null} is the mean optical density of the blank filter between 750 and 800 nm, β_{λ} is the path length amplification factor of the filter set to 2 (Bricaud and Stramski 1990; Roesler 1998), V_f is the filtered volume (m^3) and A_f is the filtration area (m^2). The same equation was applied to a_{NAP} and the values were non-linearly fitted to exclude traces of residual pigment absorption following Belzile et al. (2004) over the spectral range 380-730 nm, excluding the 400-480 and 620-710 nm ranges as in Babin et al. (2003). The total pigment absorption a_{ϕ} was then calculated by subtracting non-algal absorption from the total particulate absorption ($a_{\phi} = a_p - a_{NAP}$).

Total nitrogen (TN) samples, collected in July 2015, were fixed with H_2SO_4 (final concentration 0.1%) and stored at 4°C until analysis. Back in the laboratory, the samples were treated by alkaline persulfate digestion and analyzed by sulfanilamide colorimetry after hydrazine reduction (Lachat autoanalyzer, QuikChem® Method 12-107-04-1-E).

Biological variables

Lake water samples were fixed with glutaraldehyde (final concentration of 1% for heterotrophic bacteria and picocyanobacteria, 0.5% for viruses) and stored at -80°C until analysis. Viruses and bacteria were stained with SYBR Green I dye (ThermoFisher Scientific, Waltham, MA) and their concentrations then measured in an Accuri C6 flow cytometer (BD Biosciences, San Jose, CA). Picocyanobacteria were detected and enumerated via their red autofluorescence (channel FL4) using an Epics Altra flow cytometer (Beckman Coulter, Indianapolis, IN).

© The Author(s) or their Institution(s)

Water sampled for pigment analysis was filtered through 25 mm GF/F filters that were stored initially in the field at -20°C and then at -80°C until analysis. Microbial mats were also stored in the field at -20°C and then at -80°C until analysis. Pigments from the filters and the mats were extracted with methanol 95% and measured by high pressure liquid chromatography (HPLC) as in Bonilla et al. (2005). Four successive extractions were necessary to retrieve all the pigments from the microbial mats. Microbial mat samples contained abundant degraded chlorophylls and carotenoids. Unknown carotenoids were quantified using standard conversion factors from their closest relative according to their retention time and spectra. If the carotenoid was not closely related to a known standard, the ß,ß-carotene conversion factor was used, except for myxol-glycosides, for which we used the myxoxanthophyll conversion factor. For unknown chlorophylls, the chlorophyll *a* (Chl *a*) conversion factor was used.

Additional lake water samples were fixed with a mixture of glutaraldehyde and paraformaldehyde for protist identification as in Lovejoy et al. (1993). Heterotrophic and autotrophic protists were counted and identified in sedimentation chambers (Utermöhl 1958) with an epifluorescence microscope at 400X (Axiovert 10, Zeiss, Germany). Zooplankton samples were collected using a 21 cm diameter net (63 µm mesh), fixed with formaldehyde (final concentration 4%) and then identified and counted by light microscopy at 100X magnification.

Seston samples for fatty acid profiling were collected from the surface of the inshore (S1) and central (S4) sites on 47-mm GF/F filters. Zooplankton samples were collected with a tow net (63 µm mesh) and also preserved on GF/F filters. Seston and zooplankton samples, along with mosses, microbial mats and chironomids, were kept frozen and freeze-dried. Fatty acids were extracted following a one-step transmethylation in methanol:toluene:acetyl chloride (4000:1000:125) at 90°C for 20 min, the fatty acid methyl esters (FAMEs) were then extracted

© The Author(s) or their Institution(s)

with water and hexane, and quantified by gas chromatography-mass spectrometry (GC-MS) as described in Schneider et al. (2017). Our analyses focused on the unsaturated fatty acids C16:1n-7, C18:2n-6, C18:3n-3, C20:4n-6, C20:5n-3, C22:6n-3 and C24:1n-9 as phytoplankton biomarkers (Kelly and Scheibling 2012; Grosbois et al. 2017).

Statistical analyses

One way ANOVAs and Tukey HSD tests were performed on limnological variables according to their position in the inshore-offshore gradient. Appropriate transformations were applied to respect normality and homogeneity of variances and p-values were adjusted with the Benjamini-Hochberg procedure. Cluster analyses were performed with Euclidian distances of the limnological variables and with Bray-Curtis distances of the protist and rotifer communities as well as the pigment assemblages of the water column and the benthic microbial mats. A principal coordinate analysis (PCoA) was performed with the Bray-Curtis distance of the selected fatty acids with the *pcoa* function of the *ape* package in *R* (Borcard et al. 2011).

Results

Moat dynamics

During our sampling in July 2015, the ice cover of Ward Hunt Lake had a mean thickness of 196 cm in the intermediate under-ice site (S3) and 218 cm in the central under-ice site (S4), and the moat was approximately 20 m wide. In the warm summer of 2016, the ice in July was 180 cm thick at S4 and the moat was 30 m wide; in July 2017 the ice was 151 cm thick at S4 and the moat was 25 m wide, and in July 2018 it was 158 cm thick at S4 and the moat was 15 m wide. The first

© The Author(s) or their Institution(s)

set of camera images available on 25 June 2016 showed that the moat was already established by that date and continued to widen until the break-up of the ice over on 2 August, with complete loss of ice by 15 August and freeze-up in early September (Fig. 2a). In 2017, the first images were available on 18 July and showed a moat approximately 15 m wide that likely formed during June. As in 2016, freeze-up occurred in early September. In 2018, a full annual set of images was obtained that spanned the entire moat cycle. These show the onset of the moat on 28 June 2018, and its persistence for 67 days until freeze-up on 4 September 2018. The image archive highlights the large interannual variability in moat extent, from up to 25% of the lake surface in 2016 (before complete ice break-up), to 10% and 5% of the lake surface in 2017 and 2018, respectively (Fig. 2). Some of the images during the spring and fall period when the lake was completely ice-covered showed that the smooth moat ice was clear of snow, while snow covered the offshore lake ice (NEIGE 2020).

Physicochemical profiles

The vertical profiles of temperature, dissolved oxygen and conductivity showed pronounced changes along the inshore-offshore transect (Fig. 3). The shallow water column at S1 was fully mixed at 5.5°C, falling to 3.8°C in the surface waters at S2. At the ice-covered sites S3 and S4, a thin layer of cold meltwater below 1°C lay over the warmer water beneath (Fig. 3a), with the highest temperatures around 7.0°C, between 4 and 5 m in the water column. Oxygen concentrations were around 100% air equilibrium at S1, consistent with full exposure of the moat zone to wind-induced mixing, while the below-ice sites S3 and S4 showed a highly stratified pattern with mid-water column values up to 140% in the depth region 4 to 8 m (Fig. 3b). Specific conductivity values were low and homogenous at S1 (from 0.119 to 0.146 mS cm^{-1}), while the offshore sites showed

© The Author(s) or their Institution(s)

pronounced water column gradients, rising from 0.040 mS cm^{-1} in the dilute meltwater beneath the ice to 0.309 mS cm^{-1} at the bottom of the water column (Fig. 3c). The marginal ice site S2 showed vertical gradients in temperature, oxygen and conductivity, but these were much less pronounced than at ice-covered sites S3 and S4.

As expected, underwater light conditions varied greatly across the transect. At the ice-free site S1, 54.1% of the total incoming irradiance reached the bottom at 2 m depth, while at the ice-covered site S4, only 26.5% entered the top of the water column immediately beneath the ice, falling to 5.5% at 9.4 m (Fig. 4). The ice cover allowed a slightly greater proportion of ultraviolet radiation (UVR; 33.3% penetration) compared to PAR (27.1%); UVR at 2 m depth in the inshore moat site S1 was 48.0% of incoming UVR, but undetectable at the bottom of the water column at S4. The downward irradiance spectra and the K_d at 2.0 m showed a similar pattern at S1 and S4, with the least attenuation between 400 and 600 nm (Fig. 4). The upward irradiance spectra were strikingly different between the two sites. Wavelengths between 600 and 700 nm were reflected by the bottom in the inshore moat site (S1) and upwelling irradiance values at 2 m were higher than the upwelling values at the surface (Fig. 4). In S4, upward spectral irradiance peaked at 573 nm just below the ice (2.0 m) and near the bottom at 9.1 m (Fig. 4).

Maximal values of the diffuse extinction coefficient (K_d) were below 350 nm and over 600 nm in both the inshore and the central sites (Fig. 4). K_d was lower for wavelengths above 600 nm in the moat than in the under-ice zone. The apparent K_d of the ice (not corrected for reflection) increased toward longer wavelengths. The total K_d between 300 and 720 nm was 0.31 m^{-1} for the 2 m water column at S1 falling to 0.20 m^{-1} for the upper 2 m of the water column at S4, indicating 36% less attenuation by water under the ice. The ice cover had an apparent K_d of 0.64 m^{-1} and the water column between 2 and 9.7 m had a K_d of 0.20 m^{-1}. However, non-algal

© The Author(s) or their Institution(s)

particle and algal particle absorption values were lower inshore and CDOM absorption was almost identical in the two sites (Fig. 5a), suggesting that scattering affected the observed variations in light attenuation. Absorbance peaks at 439 nm and 674 nm associated with Chl *a*, and at 625 nm associated with phycocyanin, a characteristic cyanobacteria pigment, were more pronounced in the central site (S4).

Inshore-offshore concentration gradients

Two patterns of change along the inshore-offshore transect were observed in the measured chemical and biological properties. The first pattern consisted of an abrupt drop at S2 in the ice margin site, where Chl *a* and phytoplankton were less concentrated and total nitrogen more concentrated (Fig. 6), and where DOC, bacteria, and mixotrophic protists tended to be less concentrated. The second pattern was a shift of concentrations between the ice-free moat zone (S1, S2) and the ice-covered zone (S3, S4). Lower concentrations of viruses and higher concentrations of rotifers were observed in the inshore and ice-margin sites as opposed to the intermediate and central sub-ice sites (Fig. 6e,k).

Our survey of Ward Hunt Lake with an underwater Go-Pro video camera attached to the profiling probe in 2014 revealed an unexpectedly luxuriant community of cyanobacterial mats and mosses at the deepest site (9.7 m), and these mat communities had a higher taxonomic richness than in the moat zone mats (Mohit et al. 2017). The dominant moss species was identified as *Drepanocladus brevifolius*, and a continuous layer of chironomid tubes was also observed at S3 in the intermediate sub-ice site. Chironomid larvae were identified as *Metriocnemus* sp. and samples of the tubes averaged 1.5 cm length. Using this average as horizontal scale, we estimated a density of 14 000 tubes per m^2 from a screenshot of the underwater video (Supplementary Fig. S2). We

© The Author(s) or their Institution(s)

also observed larvae and adults in the ice, and adults on the ice surface, indicating that individuals were swimming up from their tubes and migrating through fissures in the candled ice to the atmosphere to complete their life cycle (Supplementary Fig. S2f).

Cluster analysis of all variables

According to the cluster analyses (Fig. 7), there was a clear distinction between the open-water moat (S1 and S2) and offshore ice-covered (S3 and S4) zones. The intermediate and central sites (S3 and S4) generally clustered together, suggesting more homogenous conditions under the ice. The ice-margin site was distinct relative to the others according to the limnological parameters, algal pigments in the water column and rotifer assemblages (Fig. 7).

According to their clustering, the nanoplankton communities observed by microscopy were less separated by sites than other groups. The inshore (S1) and intermediate (S3) sites were more similar to each other, with higher concentrations of *Snowella* sp., *Micractinium* sp., and *Tabellaria* sp. The central (S4) and ice-margin (S3) sites also showed similarities, with higher concentrations of *Tetraedron* sp. and *Synura* sp (Supplementary Table S1).

An unusual feature of Ward Hunt Lake was that there was no evidence of crustacean zooplankton in any of our net samples, consistent with a previous mid-summer sampling of the lake (M. Rautio, unpublished observations). However, there were abundant rotifer populations, with 10 species (Supplementary Table S2), of which four dominated. The rotifer communities at S1 in the moat zone had a greater abundance of *Ascomorpha* sp. (237 ind. m^{-3}), *Asplanchna priodonta* (128 ind. m^{-3}), and *Keratella hiemalis* (116 ind. m^{-3}; Supplementary Table S2) relative to under the ice, while the ice margin S2 samples contained the highest concentrations of *Rhinoglena* sp. (260 ind m^{-3}).

© The Author(s) or their Institution(s)

The inshore moat site (S1) water column was characterized by the presence of a pigment similar to 4-ketomyxol 2'-fucoside, which is associated with cyanobacteria, notably *Pseudanabaena* and oscillatorians (Takaichi et al. 2005; Lionard et al. 2012). Pigment assemblages in the water column at the ice margin site S2 were characterized by twice the concentrations of diadinoxanthin, peridinin and unknown myxol-glycosides compared to the other sites (Supplementary Table S3). Diadinoxanthin is associated with diatoms, peridinin with dinoflagellates, and myxol-glycosides with cyanobacteria (Roy et al. 2011).

Pigments extracted from the benthic mats at S1 were distinct from benthic mat pigments in the ice-covered zone, with higher concentrations of scytonemin and reduced scytonemin, both signature pigments of UV-exposed cyanobacteria (Bonilla et al. 2005; Roy et al. 2011). The offshore benthic mats additionally contained bacteriochlorophyll *c*, which is generally associated with green sulfur bacteria that grow under anoxic conditions (Supplementary Table S4).

Fatty acids

The highest total fatty acid (FA) concentrations were measured in the central site (S4) samples of seston and zooplankton (means of 479 and 290 μg/mg dry weight, respectively; Fig. 8a; Supplementary Table S5). Microbial mats contained the lowest concentrations (mean 25 μg/mg dry weight), especially in the inshore (S1) and central (S4) sites. Inshore organisms contained more polyunsaturated fatty acids (PUFA) than in the ice-covered zone (sites S3 and S4; Fig. 8b-f), but the distribution differed statistically only for microbial mats; due to the small sample sizes, no statistical tests were done for the mosses or chironomids. According to the PCoA performed with fatty acid assemblages (Fig. 9), pelagic (seston) and benthic (microbial mats and mosses) food sources were different from each other but showed only slight differences between the central and

© The Author(s) or their Institution(s)

inshore moat sites. Seston fatty acid assemblages were characterized by higher concentrations of C22:6n-3 that is a bioindicator for phytoplankton (Kelly and Scheibling 2012). The distribution of the assemblages in the biplot suggests a strong differentiation in zooplankton diet between the ice-free moat and under-ice zones (Fig. 8). The zooplankton fraction (>63 μm) from the central site (S4) shared a similar fatty acid profile to the seston, suggesting their main food source was located in the water column. Zooplankton from the inshore moat site (S1) contained higher concentrations of C16:1n-7, a bioindicator for diatoms but also for cyanobacteria (Taipale et al. 2015) that were both common in the microbial mats, suggesting their diet is from diverse benthic phototrophs in these mats. The fatty acid assemblages in *Metriocnemus* larvae were more heterogenous, but all were closely related to the microbial mats, indicating that these biofilms may provide food resources for these benthic consumers in the central as well as inshore sites.

Discussion

Moat development

An ice-free peripheral moat is a common feature of Antarctic and Arctic waterbodies (Adams et al. 1989; Miller and Aiken 1996), and is a distinct within-lake environment that can persist for many weeks each summer. The formation of the moat is initially rapid as a result of higher solar fluxes per unit volume in the shallow ice-free zone, the positive feedback effect of the resultant meltwater, the arrival of inflows and additionally, as indicated here, by reduced snow cover and albedo. Our observations of less snow retention over the inshore ice-free zone are consistent with those of Adams et al. (1989), who attributed this to the wind removal of snow from smoother moat ice and the accumulation of snow on rougher, slightly higher, multi-year ice.

© The Author(s) or their Institution(s)

Once the moat of open water is formed, its area then remains more stable for a prolonged period (Welch 1973), with the thermal inertia of the thicker offshore ice and deeper water column acting as a brake on the subsequent rate of ice loss. As we observed, however, there can be large variations in moat extent among years. The width of the moat of Ward Hunt Lake as estimated by the automated camera images extended from less than 5% to 25% (in September 2018 and August 2016, respectively) of the total lake area. In 2015, the width was around 20 m, similar to the moat of Lake A on nearby Ellesmere Island as measured in 2007 (Tomkins et al. 2009). This moat extent is larger than in the perennially ice-capped lakes of the McMurdo Dry Valleys of Antarctica, where the summer moats account for around 3% of total lake area (Wharton et al. 1986; Priscu et al. 1996). In these south polar lakes, as at Ward Hunt Lake, there can be large variations among years; for example, Lake Fryxell had up to 11% of open water in the 2013-2014 summer, associated with higher air temperatures (Wayt et al. 2017). In the most extreme Antarctic lakes such as Lake Untersee, no moat has been observed and the lakes remain completely sealed throughout the year (Faucher et al. 2020).

Physicochemical variables

Given the high transparency of its waters, the entire expanse of Ward Hunt Lake might be considered as a “littoral zone” according to the definition of Peters and Lodge (2009), based on light penetration to at least 1% irradiance at the bottom. However, the distinct characteristics imposed by the presence of ice results in marked, discontinuous inshore-offshore differences, from the fully exposed moat zone to the shaded ice-covered zone. The horizontal extent of the inshore open-water zone is therefore a more meaningful descriptor of spatial differences in limnological

© The Author(s) or their Institution(s)

properties of Arctic lakes that are ice-covered for most of the year than traditional definitions of the littoral zone.

The patterns observed in Ward Hunt Lake underscore the importance of ice cover as the main driver of spatial variation, with the ice edge as the key determinant of horizontal structure. The physicochemical profiles under the ice varied little among sites (Fig. 3). The ice cover allowed inverse thermal stratification along with chemical stratification by preventing exposure to the atmosphere and wind-induced mixing. Ice has a low thermal conductivity, limits heat loss in the atmosphere and allows solar heating of the water column to temperatures well above those of the overlying air: Ward Hunt Lake had under-ice water temperatures up to 7°C, yet air temperatures averaged around 1.7°C in July (Bégin et al. 2020). This greenhouse effect has been modelled in other ice-covered lakes of the Arctic (Vincent et al. 2008) and Antarctica (Obryk et al. 2019).

Complete loss of ice cover during warm summers allows mixing of the water column and ventillation of heat to the atmosphere, and water temperatures can then drop to near freezing (Schindler et al. 1974; Doran et al. 1996; Bégin et al. 2020). The vertical structure that was lost in Ward Hunt Lake in 2016 was reinstated in summer 2017 beneath the first-year ice cover, but with lower temperatures (Bégin et al. 2020). The presence of ice cover hence allows a stable and relatively warm environment to develop, which may stimulate primary production (Markager et al. 1999) and microbial food web activity (Wrona et al. 2006). However, these effects may be offset by the influence of ice in reducing light availability, mixing and nutrient supply.

High concentrations of oxygen were recorded between 4 and 9 m, indicating net autotrophy in the water column. At the bottom of the central under-ice site (S4), the oxygen concentration was around equilibrium (Fig. 3), suggesting a balance between gain and loss processes. The bottom waters of Ward Hunt Lake are well oxygenated in July, but reach anoxia at the beginning of winter

© The Author(s) or their Institution(s)

that persists until spring (Bégin et al. 2020). In contrast, frequent mixing in the ice-free moat zone likely keeps the water and the microbial mats well oxygenated until freeze-up, which translates into a lower proportion of anaerobic bacteria (Mohit et al. 2017). Concentrations of oxygen above saturation (near 200% in Ward Hunt Lake) are well documented in ice-covered lakes of high latitudes (Wharton et al. 1993; Ludlam 1996). Wharton et al. (1993) suggested two main sources for high oxygen concentrations: oxygenic photosynthesis and oxygen exclusion from newly forming ice when water from inflowing streams freezes in contact with the bottom of the ice cover.

Vertical gradients in conductivity were steeper in the ice-covered sites (Fig. 3), probably due to the cold meltwater derived from the ice cover being less concentrated in ions, and remaining at the surface without mixing with the rest of the water column because of its greater buoyancy at near-zero temperatures (Bergmann and Welch 1985). Conductivity in the water column increased along the inshore-offshore gradient, possibly due to inputs from the sediments (including weathering of catchment mineral particles), from ions released by ice formation in the preceding fall and from microbial decomposition processes. The water tracks on the western shore of the watershed are the main source of freshwater for the lake (Paquette et al. 2017). As also seen in the present study, the ionic composition of freshwaters channelled through water tracks on the western slope of Ward Hunt Lake is dominated by bicarbonate and calcium (Paquette et al. 2020). The accumulation of ions in Ward Hunt Lake could further be accelerated by the absence of mixing of low-conductivity ice-melt water with the underlying water column before it reaches the outflow, as was observed in P&N Lake on the west coast of Hudson Bay (Bergmann and Welch 1985).

As the result of the ice cover, the moat and ice-covered zones differed markedly in terms of the quantity of solar energy reaching the top and bottom of their water columns (Fig. 4). In nearby Lake A, the K_d is in these wavelengths was up to 53% lower in snow-free ice than in water, but

© The Author(s) or their Institution(s)

43% higher in the PAR waveband (Belzile et al. 2001). The penetration of green light at the bottom of the moat and ice-covered zones (notably in the range of 500 to 575 nm) observed in Ward Hunt Lake is generally common in lakes since maximal absorption for Chl *a* is at 640 and 405 nm and for Chl *b* at 620 and 440 nm, with carotenoids and CDOM also absorbing light in blue-green wavelengths and water itself absorbing strongly at the red end of the spectrum (Wetzel 2001).

There were pronounced differences in upward spectral irradiance between the moat and ice-covered zones of the lake. In the upper waters of the central under-ice site (S4), the maximal irradiance was observed between 500 and 575 nm, as for downward irradiance (Fig. 4). At the bottom, there was a shift towards a maximum at 563 nm, which indicated a selective reflection of light from the bottom at green wavelengths, and selective absorption of light at higher and lower wavelengths by microbial mat pigments. In the inshore moat site (S1), upward irradiance at wavelengths above 570 nm was higher than upward irradiance at the surface (Fig. 4), which was likely due to pigments reflecting in the orange and red part of the spectra, and confering the colour of the mats (Supplementary Fig. S2b). The inshore mats had higher concentrations of cyanobacterial pigments including 4-ketomyxol 2'-fucoside, β,β-carotene, echinenone and the UV-absorbing pigment scytonemin (Supplementary Table S4). High concentrations of carotenoids associated with cyanobacteria were previously observed in Ward Hunt Lake's inshore microbial mats, and their taxonomic analysis indicated a high proportion of the scytonemin-rich genus *Dichothrix* (Villeneuve et al. 2001). This is also in accordance with observations from the mats in Lake Hoare, Antarctica, where cyanobacterial pigments associated with high carotenoid concentrations were mainly concentrated in moat mats (Hawes and Schwarz 1999). Moreover, the light reaching the bottom of the Ward Hunt Lake inshore moat site is reduced in wavelengths lower than 400 nm, probably as a result of absorption by CDOM (Fig. 5). The lake watershed is rich in

© The Author(s) or their Institution(s)

carbonates (Trettin 1991), and the resultant light coloured rocks confer a high reflecting potential to the rock-coated moat zone (Supplementary Fig. S2a; Wetzel 2001).

The UVR attenuation coefficients (K_d) at 320, 340 and 380 nm for the first 2 m at the surface of Ward Hunt Lake were respectively 0.60, 0.47 and 0.32 m^{-1} in the inshore moat site (S1) and 0.63, 0.62 and 0.63 m^{-1} in the central site (S4; Fig. 4). These lie well below values recorded in the surface 5 m of the nearest lake, meromictic Lake A, located 20 km southwest of Ward Hunt Lake, where K_d was 1.65, 1.33, and 0.80 m^{-1} at the same wavelengths. These higher values at Lake A are likely due to higher CDOM absorbance, with its a_{CDOM} values between 2 and 3 m^{-1} at 320 nm (Belzile et al. 2001) compared to our a_{CDOM} observations of 0.69 m^{-1} in the moat and 0.78 m^{-1} in the central sites of Ward Hunt Lake. However, the K_d values for PAR (400-700 nm) in Ward Hunt Lake (0.314 and 0.209 m^{-1} for the surface waters of the inshore and central sites), and are similar to the value of 0.352 m^{-1} recorded in Lake A (Belzile et al. 2001). These K_d values are also within the range of other Arctic Lakes located on Cornwallis Island such as Meretta, Eleanor, and Char Lakes (0.24-0.39 m^{-1}; Markager et al. 1999), and are similar to the values obtained in Lake Hoare and Lake Fryxell in the McMurdo Dry Valleys (0.197, 0.214 m^{-1} at the surface), but well above those in Lake Vanda and Lake Bonney, also in the McMurdo Dry Valleys, that contain <0.7 mg DOC L^{-1} and <0.1 μg Chl *a* L^{-1} (Vincent et al. 1998).

The higher K_d spectral values in the central site (S4) of Ward Hunt Lake for the UVR portion of the spectra are coherent with higher absorption by algal and non-algal particles (Fig. 5). In 2015, the central site contained lower concentrations of nanoplankton (S1; Supplementary Table S1). However, Chl *a* concentrations were higher in the central site compared to the inshore moat site, along with higher total pigment concentrations. Hence, cells could be less abundant but cellular pigment concentrations higher as a result of photoacclimation to the low light environment

© The Author(s) or their Institution(s)

(Thompson et al. 1991). Ice cover on the central site of Ward Hunt Lake was thinner at the moment of irradiance measurements in 2016 and optical measurements in 2017 (average of 180 and 151 cm, respectively) compared to the inshore-offshore gradient sampling performed in 2015 (218 cm), and this may have contributed to some of the interannual differences in plankton and pigments.

Inshore-offshore gradients

Limnological variables followed two distinct patterns along the inshore-offshore gradient: a pronounced change at the ice margin (S2) that contrasted with the three other sites, and contrasting conditions between the ice-free and ice-covered sites (S1 and S2 versus S3 and S4). These two patterns highlight the role of ice margin as a zone of disjunction in the surface limnological properties of the lake. According to the first pattern, there was a clear decrease in concentrations of DOC, Chl *a* and mixotrophic protists in the ice-margin site (Fig. 6b,d,i). The lower concentrations observed in the ice margin site could be the result of convective upwelling. Low-density cold water released from the melting ice cover may circulate from under the ice towards the shore (Bochaton 2017). Given the homogenous physical conditions in the inshore moat site (S1), convective upwelling initiated by the warming of its water in the inshore site, as observed in Lake N2 in Alaska (Cortés and MacIntyre 2020), seems unlikely. Total nitrogen concentrations, contrary to most of the other variables, was higher at the ice margin (Fig. 6a), possibly as a result of dissolved and particulate N release from the melting ice face. However there were lower concentrations of DOC, bacteria, Chl *a*, autotrophic protists and pigments, suggesting lower primary production.

The second observed pattern included the change of concentration in viruses and rotifers between the ice-covered and the ice-free zones (Fig. 6). Viruses had lower concentrations inshore

© The Author(s) or their Institution(s)

and in the ice margin, and their increase under the ice co-occurred with higher concentrations of DOC, Chl *a* and bacteria (Fig. 6b,d,g). Viruses have the potential to short-circuit the classical food web by attacking primary producers and releasing carbon that is only available to smaller organisms in the lower part of the food web (Wilhelm and Suttle 1999). The virus to bacteria ratio (VBR) ranged from 1.8 to 3.8, which is in the lower range of the Antarctic freshwater environments described by Säwström et al. (2007). Low VBRs suggest low bacterial mortality due to viral infection and is correlated with low bacterial abundance (Wommack and Colwell 2000; Yager et al. 2001). Lower concentrations of viruses in the ice-free zones could be attributable to their vulnerability to decay via sunlight (Suttle and Chen 1992). The pattern in rotifer communities was completely the opposite, where higher concentrations were observed in the moat zone (Fig. 6k) along with a higher abundance of picocyanobacteria and autotrophic protists (Fig. 6f,h). The central site (S4) was dominated by *K. hiemalis* that feeds preferentially on bacteria and detritus. The inshore moat site (S1) was dominated by high abundances of species that feed on larger particles such as *Ascomorpha* sp. that prefers dinoflagellates, *Rhinoglena* sp. that feeds on chrysophytes and *A. priodonta* that is predatory (Supplementary Table S2; Pourriot 1977).

Some variables did not clearly follow the two patterns depicted above. Autotrophic protists were higher in the inshore moat and dropped consistently in the ice margin to stay low under the ice (Fig. 6h). Higher concentrations of phototrophs are likely associated with higher light availability, and the drop at the ice margin could be related to higher grazer concentrations (heterotroph protists and rotifers; Fig. 6j,k). The most abundant rotifer in the ice-margin site, *Rhinoglena* sp., feeds on small unicellular algae and on detritus (Ruttner-Kolisko 1974). Higher concentrations of bacteria observed in the central site (S4) could be associated with a lower predation rate by heterotrophs or higher concentrations of DOC. However, genomic analyses of

© The Author(s) or their Institution(s)

the microbial mats from the moat zone at our site S1 detected heterotrophic ciliates as the dominant eukaryotes, suggesting high microbial food web activity (Mohit et al. 2017).

Consistent with our hypothesis, there were clear discontinuities at the ice-margin site, indicating the decisive effect of ice cover in separating habitat properties between inshore and offshore parts of the lake. Lake ice margins have some characteristics in common with the edge of the sea ice in the Arctic Ocean, which is also undergoing transition from perennial to seasonal ice conditions associated with climate warming (Polyakov et al. 2012). The limnological variables at sites 3 and 4 of Ward Hunt Lake were closely similar, as was ice thickness. The ice-covered area of polar lakes thus has the potential to maintain a relatively uniform conditions, in contrast to the much more variable conditions of the moat zone. In the marginal ice zone of the Arctic Ocean, mismatches have been observed between phototrophs (ice algae and phytoplankton) and heterotrophs due to the earlier ice break up (Søreide et al. 2010). Such mismatches may also occur in Ward Hunt Lake where the phytoplankton phenology has been observed to change with complete loss of ice cover (Bégin et al. 2020).

Cluster analysis of the different biological variables confirmed the strong spatial differences. Rotifer communities clustered distinctly in the ice-free and ice-covered zones, and the communities of the inshore and ice-margin sites were in separate branches, while those in the central and intermediate sub-ice sites were merged (Fig. 7c). A clear distinction between fatty acid assemblages of zooplankton between open-water and ice-covered sites was also observed (Fig.9). Our results suggest that under the ice, zooplankton diet is more likely to be composed exclusively of seston, whereas in the inshore moat site microbial mats or epibionts associated with mosses, with their higher concentrations of PUFAs (Fig. 8), could contribute to a larger extent to zooplankton diet. Sea ice has been identified as a rich ecosystem where algae can contain higher

© The Author(s) or their Institution(s)

levels of fatty acids than phytoplankton with large proportions of PUFAs (Falk-Petersen et al. 1998), but lake ice lacks the nutrient-rich brine channels of sea ice and would seem to provide a much less suitable habitat for algal growth. Little is known, however, about the biomass and productivity of ice-associated algae in lakes (Hampton et al. 2015).

A clear distinction according to the presence of the ice cover in Ward Hunt Lake was also observable in the limnological variables, pigments of the water column and PUFAs in chironomids (Fig. 7a,e, 8 and 9), underscoring the homogeneity of response of these variables under the ice cover. The clear pattern in pigments was not reflected in the cluster of protist communities, which included autotrophs, heterotrophs and mixotrophs (Fig. 7b), nor between under-ice and moat seston fatty acid assemblages. (Fig. 8). The central sub-ice site generally contained more heterotrophs than the inshore moat site S1, mainly small-sized (<5 μm) non-flagellated heterotrophs (Supplementary Table S1). The inshore site was characterized by the highest concentrations of autotrophs, likely due to light availability, especially diatoms, colonial cyanobacteria (*Snowella* sp.) and the chlorophyte *Micractinium* sp. Mixotroph protists were generally more abundant in the intermediate site, especially *Dinobryon* sp., *Ochromonas* sp. and *Cryptomonas* sp. Additional under-ice light measurements would help to determine if ice degradation in this site could have reduced light availability, as white ice attenuates more light than candled ice (Welch et al. 1987). Lower light availability could give a competitive advantage to mixotrophic species (Jones 2000).

Our discovery of abundant tubes in the benthos, most likely produced by chironomids, suggests a sustained presence of these dipterans in the Ward Hunt Lake ecosystem and their likely participation in food web dynamics. Their migration from the tubes in the benthos, swimming up through the water column and then passing through fissures in the candled ice, is consistent with previous observations in the Arctic (Oliver 1964). The tube concentrations measured here

© The Author(s) or their Institution(s)

(14 000 m^{-2}) is at the upper range for lakes elsewhere, and likely results from numerous seasons of accumulation. Chironomid larvae have been observed in densities between 70 and 11 000 ind. m^{-2} (Hölker et al. 2015), and in laboratory experiments, they can cover up to 48% of the surface of artificial substrates (Pringle 2004). Although we were able to collect only a small number of chironomid individuals, the fatty acid analyses indicated that there was considerable variability in chironomid diet among mats, plankton and mosses. Despite their lower fatty acid concentrations compared to seston, microbial mats and mosses may be a good food source as they have a high proportion of PUFAs, especially ω3 and ω6 in the inshore moat site, which was reflected in larvae (Figs. 8 and 9; Supplementary Fig. S3), and the benthic mats could also subsidize the central sub-ice food web (Mariash et al. 2014). Chironomids display a remarkably large variety of modes of feeding, including by filtering, gathering, scraping, shredding, engulfing and piercing, and they are opportunistic in the type of prey they consume (Armitage et al. 2012). Food web analyses in Alaskan shallow lakes also suggested that chironomids may be closely linked to methane cycling, as their diet can be substantially composed of methanotrophic bacteria (Hershey et al. 2006). Methanotrophs could be a source of food for chironomids in Ward Hunt Lake as they are abundant in the central sub-ice mats (Mohit et al. 2017). Further analyses could be undertaken on samples from the lake using adducts of monounsaturated fatty acids specific to methanotrophic bacteria and mixing models adapted to fatty acid assemblages (Virtue et al. 1996; Galloway et al. 2014; Wauthy and Rautio 2020) to disentangle and quantify the contribution of food sources.

One of the key aspects of the moat environment to examine in the future is its hydrodynamic regime. At the time of the first studies on Ward Hunt Lake, the 4-m thick lake ice had been found to extend to the lake floor, and it was assumed that the moat region along the western shore constituted the entire liquid water of the lake, with a short residence time before discharge at the

© The Author(s) or their Institution(s)

outlet (Villeneuve et al. 2001). Subsequent studies with Ground Penetrating Radar, revealed a large area of the lake that extended to depths well below 4 m, as well as a thinning of the ice cover (Paquette et al. 2015). The latter would have enhanced the potential exchange of moat water with the offshore waters beneath the ice, including via density flows from water tracks entering the moat. Nonetheless, the persistent thick ice likely acts as an impediment to offshore exchange, and the moat water would have a shorter residence time than the main body of the lake, contributing to the distinctive limnological characteristics observed here.

Conclusions

The abrupt inshore-offshore changes that we observed in many limnological properties at the ice margin of Ward Hunt Lake underscore the importance of ice cover in the regulation and stabilization of conditions in polar lake ecosystems. The position of the ice edge can be considered a line of demarcation defining the zone of sharp transition in light quantity and quality reaching the bottom of the lake, and in the stability of the water column. The definitions of littoral versus pelagic zones derived from temperate lake studies are less appropriate for polar lakes, where instead the moat, ice-margin and ice-covered waters can be distinguished as limnologically distinct zones.

The ice edge shifts only slowly in position after the initial early season melting, but this is subject to climate-determined variations among years that in turn will influence the spatial organization of the lake, including its food webs. As atmospheric temperatures are increasing, the thickness, area and duration of the ice cover and the overlying snow depth on polar lakes are decreasing, including towards more frequent complete loss of ice. This will make the moat zone become a shorter-lived feature and may lessen the extent of inshore-offshore differences in the limnology of high latitude lakes.

© The Author(s) or their Institution(s)

Acknowledgements

This research a contribution to the projects ArCS II (Arctic Challenge for Sustainability II) supported by the Ministry of Education, Culture, Sports, Science and Technology, Japan, and the program NEIGE (Northern Ellesmere Island in the Global Environment) supported by the Canada First Research Excellence Fund (CFREF) program Sentinel North, the NCE ArcticNet, Centre d'études nordiques (CEN), Fonds de Recherche du Québec Nature et Technologies (FRQNT), the Natural Sciences and Engineering Research Council of Canada (NSERC), and the Northern Scientific Training Program (NSTP), with logistic support by Polar Continental Shelf Program (PCSP) and Parks Canada. The research was conducted under the terms of Nunavut Research Institute Science Licenses (0202615R-M, 0200316R-M, 0201917R-M, 0202118R-M, 0202519R-M) and Parks Canada Research and Collection Permits (QUT-201518856, QUT-201724479, QUT-201931997) to Warwick F. Vincent. We wish to thank Denis Sarrazin, Myriam Labbé, Michel Paquette, Nicolas Bochaton and Jérôme Comte for assistance in the field. We also thank Marie-Josée Martineau for her help with HPLC analysis, Anna Przytulska-Bartosiewicz and Marie Parenteau for support in microscopic analyses of phytoplankton, Pierre Carrier-Corbeil, Balla Sylla and Maxime Wauthy for support with fatty acids analyses, Catherine La Farge for moss identifications and Andrew S. Medeiros for chironomid larvae identification.

© The Author(s) or their Institution(s)

References

Adams, W.P., Doran, P.T., Ecclestone, M., Kingsbury, C.M., and Allan, C.J. 1989. A rare second year - lake ice cover in the Canadian High Arctic. Arctic **42**: 299–306. doi: 10.14430/arctic1670.

Armitage, P.D., Pinder, L.C., and Cranston, P.S. 2012. The Chironomidae: biology and ecology of non-biting midges, Springer Science & Business Media.

Ask, J., Karlsson, J., Persson, L., Ask, P., Byström, P., and Jansson, M. 2009. Whole-lake estimates of carbon flux through algae and bacteria in benthic and pelagic habitats of clear-water lakes. Ecology **90**: 1923–1932. doi: 10.1890/07-1855.1.

Babin, M., Stramski, D., Ferrari, G.M., Claustre, H., Bricaud, A., Obolensky, G., and Hoepffner, N. 2003. Variations in the light absorption coefficients of phytoplankton, nonalgal particles, and dissolved organic matter in coastal waters around Europe. J. Geophys. Res. **108**: C7. doi: 10.1029/2001JC000882.

Bégin, P.N., Tanabe, Y., Kumagai, M., Culley, A.I., Paquette, M., Sarrazin, D., Uchida, M., and Vincent, W.F. 2020. Extreme warming and regime shift toward amplified interannual variability in a far northern lake. Limnol. Oceanogr. **65**. doi: 10.1002/lno.11546.

Belzile, C., Vincent, W.F., Gibson, J.A.E., and Van Hove, P. 2001. Bio-optical characteristics of the snow, ice, and water column of a perennially ice-covered lake in the High Arctic. Can. J. Fish. Aquat. Sci. **58**: 2405–2418. doi: 10.1139/cjfas-58-12-2405.

Belzile, C., Vincent, W.F., Howard-Williams, C., Hawes, I., James, M.R., Kumagai, M., and Roesler, C.S. 2004. Relationships between spectral optical properties and optically active substances in a clear oligotrophic lake. Water Resour. Res. **40**: W12512. doi:

© The Author(s) or their Institution(s)

10.1029/2004wr003090.

Bergmann, M.A., and Welch, H.E. 1985. Spring meltwater mixing in small Arctic lakes. Can. J. Fish. Aquat. Sci. **42**: 1789–1798. doi: 10.1139/f85-224.

Bochaton, N. 2017. Simulated heat storage in Canada's most northern lake: Towards a 3 dimensional model. Master's Thesis. École polytechnique fédérale de Lausanne, Lausanne, Switzerland..

Bonilla, S., Villeneuve, V., and Vincent, W.F. 2005. Benthic and planktonic algal communities in a High Arctic lake: Pigment structure and contrasting responses to nutrient enrichment. J. Phycol. **41**: 1120–1130. doi: 10.1111/j.1529-8817.2005.00154.x.

Borcard, D., Gillet, F., and Legendre, P. 2011. Numerical Ecology with R, Springer.

Bricaud, A., and Stramski, D. 1990. Spectral absorption coefficients of living phytoplankton and nonalgal biogenous matter: A comparison between the Peru upwelling areaand the Sargasso Sea. Limnol. Oceanogr. **35**: 562–582. doi: 10.4319/lo.1990.35.3.0562.

CEN. 2020. Climate station data from Northern Ellesmere Island in Nunavut, Canada, v. 1.7 (2002-2019). Nordicana **D1**. doi: 10.5885/44985SL-8F203FD3ACCD4138.

Cortés, A., and MacIntyre, S. 2020. Mixing processes in small arctic lakes during spring. Limnol. Oceanogr. **65**: 260–288. doi: 10.1002/lno.11296.

Doran, P.T., McKay, C.P., Adams, W.P., English, M.C., Wharton Jr, R.A., and Meyer, M.A. 1996. Climate forcing and thermal feedback of residual lake-ice covers in the high Arctic. Limnol. Oceanogr. **41**: 839–848. doi: 10.4319/lo.1996.41.5.0839.

Falk-Petersen, S., Sargent, J.R., Henderson, J., Hegseth, E.N., Hop, H., and Okolodkov, Y.B. 1998. Lipids and fatty acids in ice algae and phytoplankton from the Marginal Ice Zone in the Barents

© The Author(s) or their Institution(s)

Sea. Polar Biol. **20**: 41–47. doi: 10.1007/s003000050274.

Faucher, B., Lacelle, D., Fisher, D.A., Weisleitner, K., and Andersen, D.T. 2020. Modeling δD-$\delta^{18}O$ steady-state of well-sealed perennially ice-covered lakes and their recharge source: Examples from Lake Untersee and Lake Vostok, Antarctica. Front. Earth Sci. **8**. doi: 10.3389/feart.2020.00220.

Galloway, A.W.E., Taipale, S.J., Hiltunen, M., Peltomaa, E., Strandberg, U., Brett, M.T., and Kankaala, P. 2014. Diet-specific biomarkers show that high-quality phytoplankton fuels herbivorous zooplankton in large boreal lakes. Freshw. Biol. **59**: 1902–1915. doi: 10.1111/fwb.12394.

Glew, J.R. 1991. Miniature gravity corer for recovering short sediment cores. J. Paleolimnol. **5**: 285–287. doi: 10.1007/BF00200351.

Grosbois, G., Mariash, H., Schneider, T., and Rautio, M. 2017. Under-ice availability of phytoplankton lipids is key to freshwater zooplankton winter survival. Sci. Rep. **7**: 11543. doi: 10.1038/s41598-017-10956-0.

Hall, C.M., Castro, M.C., Kenig, F., and Doran, P.T. 2017. Constraining the recent history of the perennially ice-covered Lake Bonney, East Antarctica using He, Kr and Xe concentrations. Geochim. Cosmochim. Acta **209**: 233–253. doi: 10.1016/j.gca.2017.04.023.

Hampton, S.E., Moore, M.V., Ozersky, T., Stanley, E.H., Polashenski, C.M., and Galloway, A.W.E. 2015. Heating up a cold subject: prospects for under-ice plankton research in lakes. J. Plankton Res. **37**: 277–284. doi: 10.1093/plankt/fbv002.

Harfmann, J., Kurobe, T., Bergamaschi, B., Teh, S., and Hernes, P. 2019. Plant detritus is selectively consumed by estuarine copepods and can augment their survival. Sci. Rep. **9**: 9076.

© The Author(s) or their Institution(s)

doi: 10.1038/s41598-019-45503-6.

Hawes, I., and Schwarz, A.M. 1999. Photosynthesis in an extreme shade environment: Benthic microbial mats from Lake Hoare, a permanently ice-covered Antarctic lake. J. Phycol. **35**: 448–459. doi: 10.1046/j.1529-8817.1999.3530448.x.

Helms, J.R., Stubbins, A., Ritchie, J.D., Minor, E.C., Kieber, D.J., and Mopper, K. 2008. Absorption spectral slopes and slope ratios as indicators of molecular weight, source, and photobleaching of chromophoric dissolved organic matter. Limnol. Oceanogr. **53**: 955–969. doi: 10.4319/lo.2008.53.3.0955.

Hershey, A.E., Beaty, S., Fortino, K., Kelly, S., Keyse, M., Luecke, C., O'Brien, W.J., and Whalen, S.C. 2006. Stable isotope signatures of benthic invertebrates in arctic lakes indicate limited coupling to pelagic production. Limnol. Oceanogr. **51**: 177–188. doi: 10.4319/lo.2006.51.1.0177.

Hölker, F., Vanni, M.J., Kuiper, J.J., and others. 2015. Tube-dwelling invertebrates: tiny ecosystem engineers have large effects in lake ecosystems. Ecol. Monogr. **85**: 333–351. doi: 10.1890/14-1160.1.

Jones, R.I. 2000. Mixotrophy in planktonic protists: an overview. Freshw. Biol. **45**: 219–226. doi: 10.1046/j.1365-2427.2000.00672.x.

Jones, R.I., Grey, J., Sleep, D., and Quarmby, C. 1998. An assessment, using stable isotopes, of the importance of allochthonous organic carbon sources to the pelagic food web in Loch Ness. Proc. R. Soc. Lond. B Biol. Sci. **265**: 105–110. doi: 10.1098/rspb.1998.0270.

Kelly, J.R., and Scheibling, R.E. 2012. Fatty acids as dietary tracers in benthic food webs. Mar. Ecol. Prog. Ser. **446**: 1–22. doi: 10.3354/meps09559.

© The Author(s) or their Institution(s)

Kishino, M., Takahashi, M., Okami, N., and Ichimura, S. 1985. Estimation of the spectral absorption coefficients of phytoplankton in the sea. Bull. Mar. Sci. **37**: 634–642.

Lionard, M., Pequin, B., Lovejoy, C., and Vincent, W.F. 2012. Benthic cyanobacterial mats in the high Arctic: multi-layer structure and fluorescence responses to osmotic stress. Front. Microbiol. **3**: 140. doi: 10.3389/fmicb.2012.00140.

Lovejoy, C., Vincent, W.F., Frenette, J.J., and Dodson, J.J. 1993. Microbial gradients in a turbid estuary: Application of a new method for protozoan community analysis. Limnol. Oceanogr. **38**: 1295–1303. doi: 10.4319/lo.1993.38.6.1295.

Ludlam, S.D. 1996. The comparative limnology of high arctic, coastal, meromictic lakes. J. Paleolimnol. **16**: 111–131. doi: 10.1007/BF00176931.

Mariash, H.L., Devlin, S.P., Forsström, L., Jones, R.I., and Rautio, M. 2014. Benthic mats offer a potential subsidy to pelagic consumers in tundra pond food webs. Limnol. Oceanogr. **59**: 733–744. doi: 10.4319/lo.2014.59.3.0733.

Markager, S., Vincent, W.F., and Tang, E.P.Y. 1999. Carbon fixation by phytoplankton in high Arctic lakes: Implications of low temperature for photosynthesis. Limnol. Oceanogr. **44**: 597–607. doi: 10.4319/lo.1999.44.3.0597.

Miller, L.G., and Aiken, G.R. 1996. Effects of glacial meltwater inflows and moat freezing on mixing in an ice-covered Antarctic lake as interpreted from stable isotope and tritium distributions. Limnol. Oceanogr. **41**: 966–976. doi: 10.4319/lo.1996.41.5.0966.

Mitchell, B.G., Kahru, M., Wieland, J., Stramska, M., and Mueller, J.L. 2002. Determination of spectral absorption coefficients of particles, dissolved material and phytoplankton for discrete water samples. Ocean Opt. Protoc. Satell. Ocean Color Sens. Valid. Revis. **3**: 231.

© The Author(s) or their Institution(s)

Mohit, V., Culley, A., Lovejoy, C., Bouchard, F., and Vincent, W.F. 2017. Hidden biofilms in a far northern lake and implications for the changing Arctic. npj Biofilms Microbiomes **3**: 17. doi: 10.1038/s41522-017-0024-3.

NEIGE. 2020. Dynamics of ice cover over a far northern lake: Direct observations of Ward Hunt Lake, Canadian High Arctic, by automated camera, v. 1.1 (2016-2019). Nord. D74. doi: 10.5885/45648CE-1A9AB63DFF91440B.

Obryk, M.K., Doran, P.T., and Priscu, J.C. 2019. Prediction of ice-free conditions for a perennially ice-covered Antarctic lake. J. Geophys. Res. Earth Surf. **124**: 686–694. doi: 10.1029/2018JF004756.

Oliver, D.R. 1964. A limnological investigation of a large Arctic lake, Nettilling Lake, Baffin Island. Arctic **17**: 69–83. doi: 10.14430/arctic3488.

Paquette, M., Fortier, D., Mueller, D.R., Sarrazin, D., and Vincent, W.F. 2015. Rapid disappearance of perennial ice on Canada's most northern lake. Geophys. Res. Lett. **42**: 1433–1440. doi: 10.1002/2014GL062960.

Paquette, M., Fortier, D., and Vincent, W.F. 2017. Water tracks in the High Arctic: A hydrological network dominated by rapid subsurface flow through patterned ground. Arct. Sci. **3**: 334–353. doi: 10.1139/as-2016-0014.

Paquette, M., Fortier, D., Lafrenière, M., and Vincent, W.F. 2020. Periglacial slopewash dominated by solute transfers and subsurface erosion on a High Arctic slope. Permafr. Periglac. Process. doi: 10.1002/ppp.2066.

Peters, J.A., and Lodge, M.D. 2009. Littoral zone. *In* Encyclopedia of Inland Waters, vol 1. *Edited by* G.E. Likens. Elsevier, Oxford, pp 79–87.

© The Author(s) or their Institution(s)

Polyakov, I.V., Walsh, J.E., and Kwok, R. 2012. Recent changes of Arctic multiyear sea ice coverage and the likely causes. Bull. Am. Meteorol. Soc. **93**: 145–151. doi: 10.1175/BAMS-D-11-00070.1.

Pourriot, R. 1977. Food and feeding habits of Rotifera. Arch. Für Hydrobiol. Beih. Ergeb. Limnol. **8**: 243–260.

Pringle, C.M. 2004. Effects of chironomid (Insecta: Diptera) tube-building activities on stream diatom communities. J. Phycol. **21**: 185–194. doi: 10.1111/j.0022- 3646.1985.00185.x.

Priscu, J.C., Downes, M.T., and McKay, C.P. 1996. Extreme supersaturation of nitrous oxide in a poorly ventilated Antarctic lake. Limnol. Oceanogr. **41**: 1544–1551. doi: 10.4319/lo.1996.41.7.1544.

Rautio, M., Mariash, H., and Forsström, L. 2011. Seasonal shifts between autochthonous and allochthonous carbon contributions to zooplankton diets in a subarctic lake. Limnol. Oceanogr. **56**: 1513–1524. doi: 10.4319/lo.2011.56.4.1513.

Roesler, C.S. 1998. Theoretical and experimental approaches to improve the accuracy of particulate absorption coefficients derived from the quantitative filter technique. Limnol. Oceanogr. **43**: 1649–1660. doi: 10.4319/lo.1998.43.7.1649.

Roy, S., Llewellyn, C.A., Egeland, E.S., and Johnsen, G. 2011. Phytoplankton pigments: characterization, chemotaxonomy and applications in oceanography, Cambridge University Press.

Ruttner-Kolisko, A. 1974. Plankton rotifers biology and taxonomy. Binnengewässer **26**: 1–146.

Sand-Jensen, K., Riis, T., Markager, S., and Vincent, W.F. 1999. Slow growth and decomposition of mosses in Arctic lakes. Can. J. Fish. Aquat. Sci. **56**: 388–393. doi: 10.1139/cjfas-56-3-388.

© The Author(s) or their Institution(s)

Säwström, C., Laybourn-Parry, J., Granéli, W., and Anesio, A.M. 2007. Heterotrophic bacterial and viral dynamics in Arctic freshwaters: Results from a field study and nutrient-temperature manipulation experiments. Polar Biol. **30**: 1407–1415. doi: 10.1007/s00300-007-0301-3.

Schindler, D.W., Welch, H.E., Kalff, J., Brunskill, G.J., and Kritsch, N. 1974. Physical and chemical limnology of Char Lake, Cornwallis Island (75° N Lat.). J. Fish. Res. Board Can. **31**: 585–607. doi: 10.1139/f74-092.

Schneider, T., Grosbois, G., Vincent, W.F., and Rautio, M. 2017. Saving for the future: Pre-winter uptake of algal lipids supports copepod egg production in spring. Freshw. Biol. **62**: 1063–1072. doi: 10.1111/fwb.12925.

Solomon, C.T., Carpenter, S.R., Clayton, M.K., Cole, J.J., Coloso, J.J., Pace, M.L., Vander Zanden, M.J., and Weidel, B.C. 2011. Terrestrial, benthic, and pelagic resource use in lakes: Results from a three-isotope Bayesian mixing model. Ecology **92**: 1115–1125. doi: 10.1890/10-1185.1.

Søreide, J.E., Leu, E., Berge, J., Graeve, M., and Falk-Petersen, S. 2010. Timing of blooms, algal food quality and *Calanus glacialis* reproduction and growth in a changing Arctic. Glob. Change Biol. **16**: 3154–3163. doi: 10.1111/j.1365-2486.2010.02175.x.

Strayer, D.L., and Findlay, S.E.G. 2010. Ecology of freshwater shore zones. Aquat. Sci. **72**: 127–163. doi: 10.1007/s00027-010-0128-9.

Suttle, C.A., and Chen, F. 1992. Mechanisms and rates of decay of marine viruses in seawater. Appl. Environ. Microbiol. **58**: 3721–3729.

Taipale, S.J., Peltomaa, E., Hiltunen, M., Jones, R.I., Hahn, M.W., Biasi, C., and Brett, M.T. 2015. Inferring phytoplankton, terrestrial plant and bacteria bulk $\delta^{13}C$ values from compound specific analyses of lipids and fatty acids. PLoS One **10**: e0133974. doi:

© The Author(s) or their Institution(s)

10.1371/journal.pone.0133974.

Takaichi, S., Mochimaru, M., Maoka, T., and Katoh, H. 2005. Myxol and 4-ketomyxol 2′-fucosides, not rhamnosides, from *Anabaena* sp. PCC 7120 and *Nostoc punctiforme* PCC 73102, and proposal for the biosynthetic pathway of carotenoids. Plant Cell Physiol. **46**: 497–504. doi: 10.1093/pcp/pci049.

Thompson, P.A., Harrison, P.J., and Parslow, J.S. 1991. Influence of irradiance on cell volume and carbon quota for ten species of marine phytoplankton. J. Phycol. **27**: 351–360. doi: 10.1111/j.0022-3646.1991.00351.x.

Tomkins, J.D., Lamoureux, S.F., Antoniades, D., and Vincent, W.F. 2009. Sedimentary pellets as an ice-cover proxy in a High Arctic ice-covered lake. J. Paleolimnol. **41**: 225–242. doi: 10.1007/s10933-008-9255-x.

Traving, S.J., Rowe, O., Jakobsen, N.M., Sørensen, H., Dinasquet, J., Stedmon, C.A., Andersson, A., and Riemann, L. 2017. The effect of increased loads of dissolved organic matter on estuarine microbial community composition and function. Front. Microbiol. **8**: 351. doi: 10.3389/fmicb.2017.00351.

Trettin, H.P. 1991. Geology of the Innuitian Orogen and Arctic Platform of Canada and Greenland, Geological Survey of Canada.

Utermöhl, H. 1958. The improvement of quantitative phytoplankton methodology. Mitt.-Int. Verein. Theor. Ang. Limnol. **9**: 1-38.

Vadeboncoeur, Y., Peterson, G., Vander Zanden, M.J., and Kalff, J. 2008. Benthic algal production across lake size gradients: Interactions among morphometry, nutrients, and light. Ecology **89**: 2542–2552. doi: 10.1890/07-1058.1.

© The Author(s) or their Institution(s)

Vander Zanden, M.J., and Vadeboncoeur, Y. 2020. Putting the lake back together 20 years later: What in the benthos have we learned about habitat linkages in lakes? Inland Waters **10**: doi: 10.1080/20442041.2020.1712953.

Villeneuve, V., Vincent, W.F., and Komárek, J. 2001. Community structure and microhabitat characteristics of cyanobacterial mats in an extreme High Arctic environment: Ward Hunt Lake. Nova Hedw. Beiheft **123**: 199–224.

Vincent, A.C., Mueller, D.R., and Vincent, W.F. 2008. Simulated heat storage in a perennially ice-covered high Arctic lake: Sensitivity to climate change. J. Geophys. Res. Oceans **113**: C04036. doi: 10.1029/2007jc004360.

Vincent, W.F., Canário, J., and Boike, J. 2019. Understanding the terrestrial effects of Arctic sea ice decline, Eos **100**. doi: 10.1029/2019EO128471.

Vincent, W.F., Rae, R., Laurion, I., Howard-Williams, C., and Priscu, J.C. 1998. Transparency of Antarctic ice-covered lakes to solar UV radiation. Limnol. Oceanogr. **43**: 618–624. doi: 10.4319/lo.1998.43.4.0618.

Virtue, P., Nichols, P.D., and Boon, P.I. 1996. Simultaneous estimation of microbial phospholipid fatty acids and diether lipids by capillary gas chromatography. J. Microbiol. Methods **25**: 177–185. doi: 10.1016/0167-7012(95)00095-X.

Wauthy, M., and Rautio, M. 2020. Permafrost thaw stimulates primary producers but has a moderate effect on primary consumers in subarctic ponds. Ecosphere **11**. doi: 10.1002/ecs2.3099.

Wayt, M.E., Myers, K.F., and Doran, P. 2017. Moat development and evolution on a perennially ice-covered lake in East Antarctica. American Geophysical Union, Fall Meeting 2017, Abstract

© The Author(s) or their Institution(s)

#C23C-1234.

Welch, H.E.J. 1973. Emergence of Chironomidae (Diptera) from Char Lake, Resolute Northwest Territories. Can. J. Zool. **51**: 1113–1123. doi: 10.1139/z73-162.

Welch, H.E., Legault, J.A., and Bergmann, M.A. 1987. Effects of snow and ice on the annual cycles of heat and light in Saqvaqjuac lakes. Can. J. Fish. Aquat. Sci. **44**: 1451–1461. doi: 10.1139/f87-174.

Wetzel, R.G. 2001. Limnology: Lake and river ecosystems, 3rd ed. Elsevier.

Wharton, R.A.J., McKay, C.P., Simmons, G.M., and Parker, B.C. 1986. Oxygen budget of a perennially ice-covered Antarctic lake. Limnol. Oceanogr. **31**: 437–443. doi: 10.4319/lo.1986.31.2.0437.

Wharton, R.A.Jr., Mckay, C.P., Clow, G.D., and Andersen, D.T. 1993. Perennial ice covers and their influence on Antarctic lake ecosystems. *In* Physical and Biogeochemical Processes in Antarctic Lakes. *Edited by* W.J. Green and E.I. Friedman. pp 53-70. doi: 10.1029/AR059p0053.

Wilhelm, S.W., and Suttle, C.A. 1999. Viruses and nutrient cycles in the sea: Viruses play critical roles in the structure and function of aquatic food webs. BioScience **49**: 781–788. doi: 10.2307/1313569.

Williamson, C.E., Saros, J.E., Vincent, W.F., and Smol, J.P. 2009. Lakes and reservoirs as sentinels, integrators, and regulators of climate change. Limnol. Oceanogr. **54**: 2273–2282. doi: 10.4319/lo.2009.54.6_part_2.2273.

Wommack, K.E., and Colwell, R.R. 2000. Virioplankton: Viruses in aquatic ecosystems. Microbiol. Mol. Biol. Rev. **64**: 69. doi: 10.1128/MMBR.64.1.69-114.2000.

© The Author(s) or their Institution(s)

Wrona, F.J., Prowse, T.D., Reist, J.D., Hobbie, J.E., Lévesque, L.M.J., and Vincent, W.F. 2006. Climate change effects on aquatic biota, ecosystem structure and function. Ambio **35**: 359–369. doi: 10.1579/0044-7447(2006)35[359:CCEOAB]2.0.CO;2.

Yager, P.L., Connelly, T.L., Mortazavi, B., Wommack, K.E., Bano, N., Bauer, J.E., Opsahl, S., and Hollibaugh, J.T. 2001. Dynamic bacterial and viral response to an algal bloom at subzero temperatures. Limnol. Oceanogr. **46**: 790–801. doi: 10.4319/lo.2001.46.4.079

© The Author(s) or their Institution(s)

List of Figures

Figure 1. Sampling along the inshore-offshore transect in Ward Hunt Lake. The black arrows show the sampling locations in the ice-free moat zone (S1, the inshore moat site; S2, the ice-margin site) and in the ice-covered zone (S3, the intermediate sub-ice site; S4, the central sub-ice site). The red arrows represent the inshore-offshore transect.

Figure 2. Images of Ward Hunt Lake captured by an automated camera located on its western shore. The full record of images and video sequences is archived in NEIGE (2020).

Figure 3. Profile gradients along the inshore-offshore transect of Ward Hunt Lake: a) temperature, b) specific conductivity and c) dissolved oxygen. Profiles were recorded on 13 July (c and d) and 19 July (a and b), 2015. Oxygen concentrations in the lake are expressed as % air-equilibrium. S1 was the inshore moat site, S2 the ice margin site, S3 the intermediate sub-ice site, and S4 the central sub-ice site.

Figure 4. Irradiance profiles at the inshore moat site (S1, 15 July 2016) and the central under-ice site (S4, 14 July 2016) of Ward Hunt Lake. Total irradiance values are for downward irradiance integrated across wavebands, expressed as percent incident downward irradiance (note the logarithmic scale). Downward irradiance (DI) is expressed as percent of downward irradiance recorded just below the surface (JBS) of the open water at S1, or just below the ice (JBI) at S4; upward irradiance (UI) is expressed as percent upward irradiance at JBS (S1) or JBI (S4). The diffuse attenuation coefficients (K_d) are for the upper 2 m of the water column at each site, and for the ice-cover at S4, uncorrected for reflection.

© The Author(s) or their Institution(s)

Figure 5. Spectral absorption coefficients for Ward Hunt Lake water samples. The coefficients are for: a) CDOM, $a_{CDOM}(\lambda)$; b) non-algal particles, $a_{NAP}(\lambda)$; and c) algal particles, $a_{\phi}(\lambda)$. The samples were from the upper water column at sites S1 and S4. The shading represents ±SE for triplicate samples.

Figure 6. Limnological gradients along the inshore-offshore transect in Ward Hunt Lake, July 2015. Values are means and SE for triplicates; different letters represent significant differences between the sites according to a Tukey HSD multiple comparison following a significant ANOVA. Results of the ANOVA comparisons of sites: a) Total nitrogen: $F_{3,8} = 5.75$, $P = 0.047$; b) Dissolved organic carbon (DOC): $F_{3,8} = 4.57$, $P = 0.060$; c) Dissolved inorganic carbon (DIC): $F_{3,8} = 3.26$, $P = 0.098$; d) Chlorophyll *a*: $F_{3,7} = 6.62$, $P = 0.047$; e) Viruses: $F_{3,8} = 5.87$; $P = 0.047$; f) Picocyanobacteria: $F_{3,8} = 1.39$, $P = 0.315$; g) Bacteria: $F_{3,8} = 5.06$, $P = 0.054$; h) Phytoplankton: $F_{3,8} = 6.166$, $P = 0.047$; i) Mixotrophic protists: $F_{3,8} = 3.58$, $P = 0.091$; j) Heterotrophic protists: $F_{3,8} = 1.97$, $P = 0.218$; k) Rotifers: $F_{3,8} = 58.28$, $P < 0.001$.

Figure 7. Cluster analysis of limnological variables, biological communities and pigments along the inshore-offshore transect in Ward Hunt Lake, July 2015. Dendrograms represent Ward clustering performed on the following distance matrices: standardized Euclidian distances for limnological variables and Bray-Curtis distances for nanoplankton, rotifers and pigment assemblages. Points filled with gray denote sites covered by ice.

Figure 8. Fatty acid methyl esters (FAME) in samples from Ward Hunt Lake at the inshore moat (S1, in white), intermediate under-ice (S3, in grey) and central under-ice (S4, in black) sites: a) total FAME concentration in µg/mg dry weight; proportion of polyunsaturated fatty acids (PUFA) in b) microbial mats, c) mosses, d) chironomid larvae, e) seston, and f) zooplankton,

© The Author(s) or their Institution(s)

expressed as percent of total FAME in their respective zones. Values are means for triplicates with SE, except for inshore mats and chironomids (n=2) and central chironomid larvae (n=1). Results of the ANOVA comparisons of total FAME: in food web compartments in panel a) $F_{4,22}$=5.75, P=0.02; in mats in panel b) $F_{2,6}$=16.85, P=0.003; in seston in panel e) $F_{1,5}$=2.77, P=0.16; and in zooplankton in panel f) $F_{1,5}$=2.65, P=0.20. Chironomid larvae were not tested due to insufficient numbers of samples.

Figure 9. Principal coordinate analysis (PCoA) of fatty acids in the Ward Hunt Lake food web. Samples were from the inshore moat (S1), intermediate under-ice (S3) and central under-ice (S4) sites. Arrows represent the contribution of the five most influential fatty acids for the distribution of samples. *Length of the C16:1n-7 arrow was divided by 3.

© The Author(s) or their Institution(s)

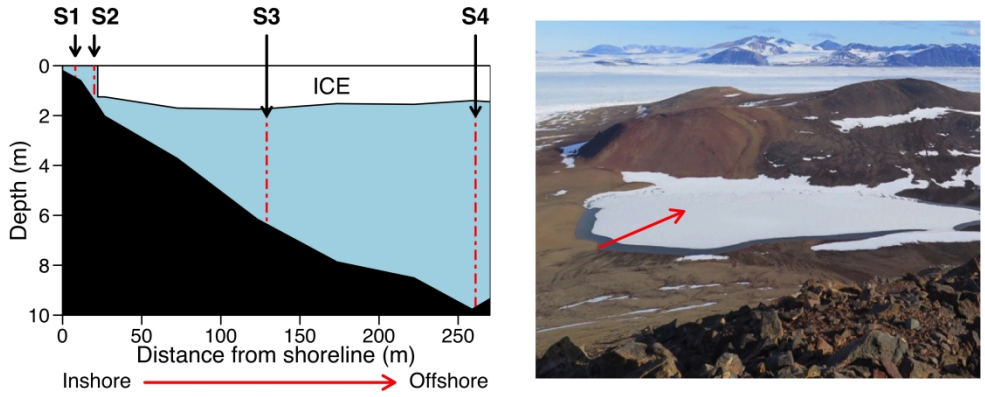

Figure 1. Sampling along the inshore-offshore transect in Ward Hunt Lake. The black arrows show the sampling locations in the ice-free moat zone (S1, the inshore moat site; S2, the ice-margin site) and in the ice-covered zone (S3, the intermediate sub-ice site; S4, the central sub-ice site). The red arrows represent the inshore-offshore transect.

1534x635mm (72 x 72 DPI)

© The Author(s) or their Institution(s)

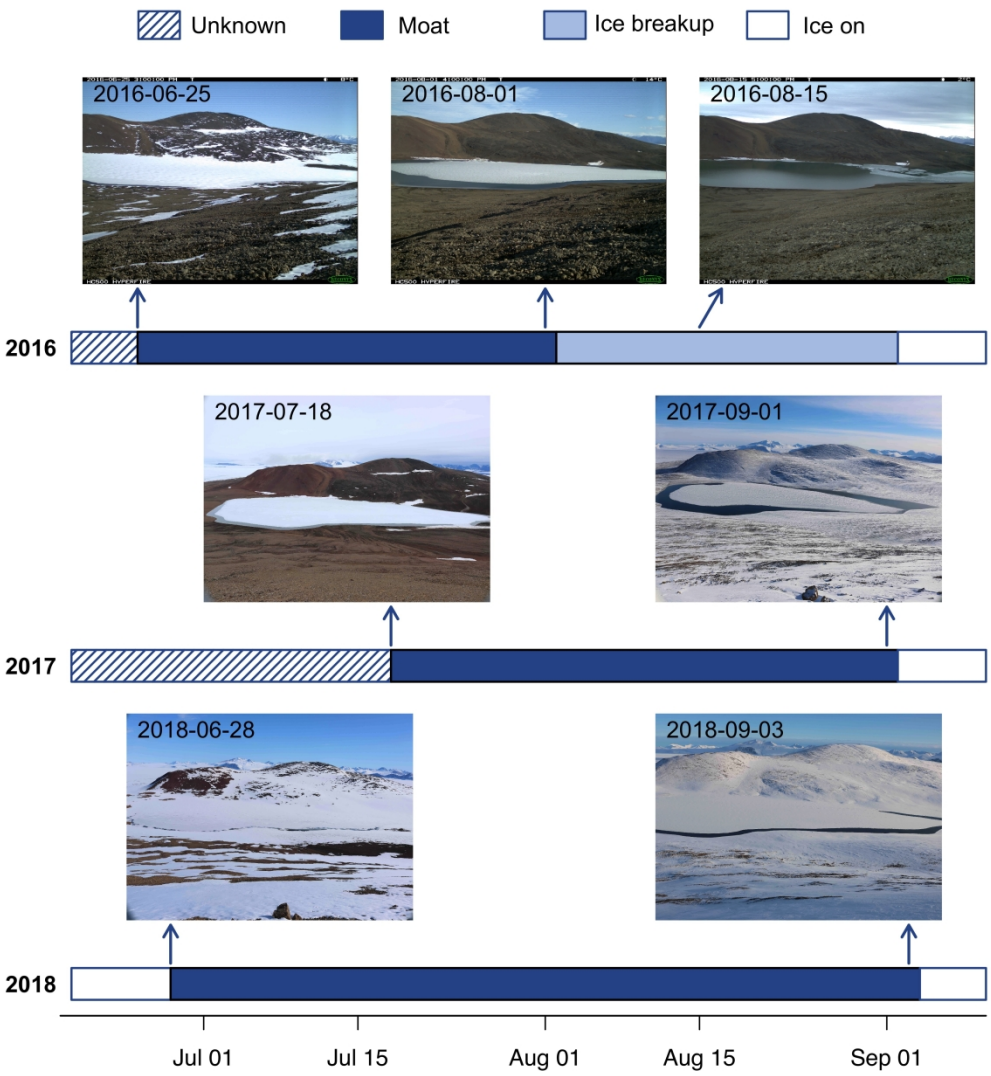

Figure 2. Images of Ward Hunt Lake captured by an automated camera located on its western shore. The full record of images and video sequences is archived in NEIGE (2020).

1534x1693mm (72 x 72 DPI)

© The Author(s) or their Institution(s)

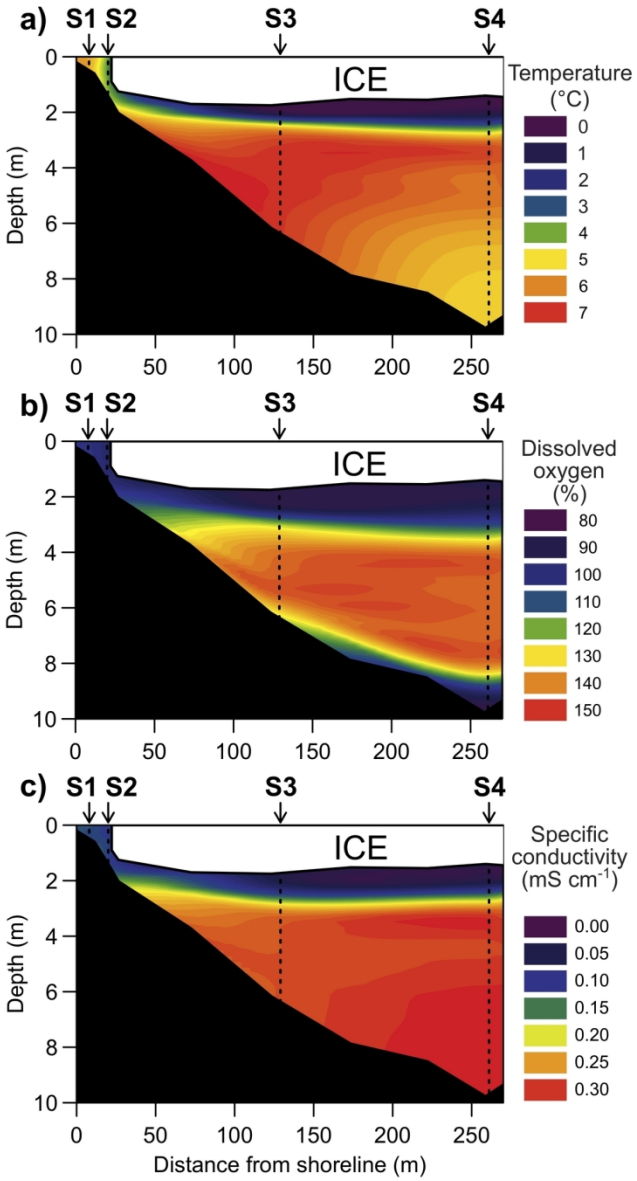

Figure 3. Profile gradients along the inshore-offshore transect of Ward Hunt Lake: a) temperature, b) specific conductivity and c) dissolved oxygen. Profiles were recorded on 13 July (c and d) and 19 July (a and b), 2015. Oxygen concentrations in the lake are expressed as % air-equilibrium. S1 was the inshore moat site, S2 the ice margin site, S3 the intermediate sub-ice site, and S4 the central sub-ice site.

101x190mm (300 x 300 DPI)

© The Author(s) or their Institution(s)

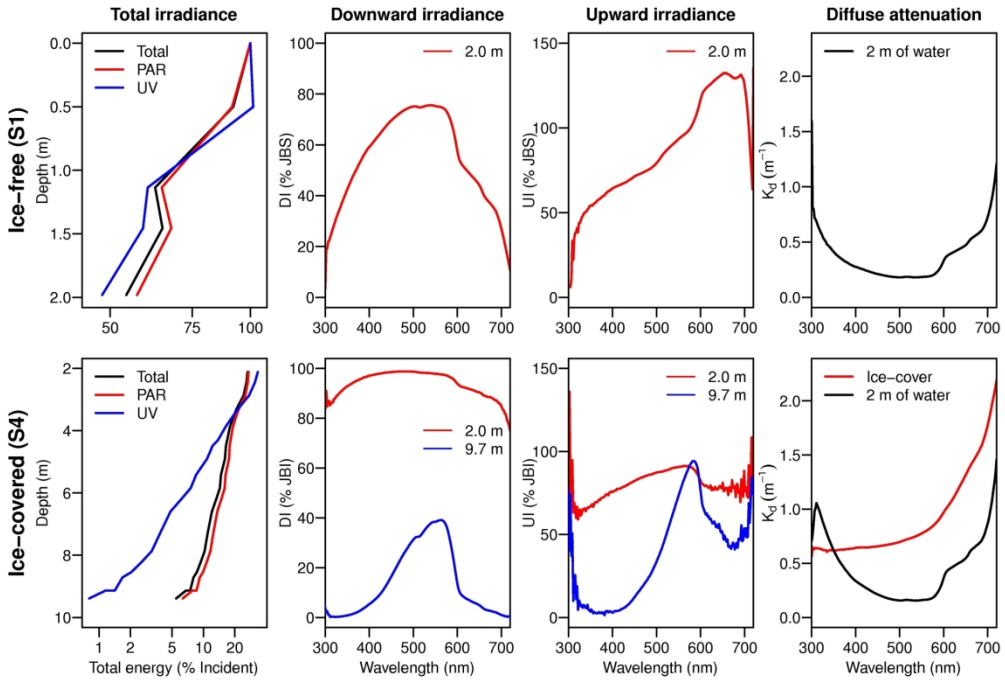

Figure 4. Irradiance profiles at the inshore moat site (S1, 15 July 2016) and the central under-ice site (S4, 14 July 2016) of Ward Hunt Lake. Total irradiance values are for downward irradiance integrated across wavebands, expressed as percent incident downward irradiance (note the logarithmic scale). Downward irradiance (DI) is expressed as percent of downward irradiance recorded just below the surface (JBS) of the open water at S1, or just below the ice (JBI) at S4; upward irradiance (UI) is expressed as percent upward irradiance at JBS (S1) or JBI (S4). The diffuse attenuation coefficients (K_d) are for the upper 2 m of the water column at each site, and for the ice-cover at S4, uncorrected for reflection.

184x127mm (300 x 300 DPI)

© The Author(s) or their Institution(s)

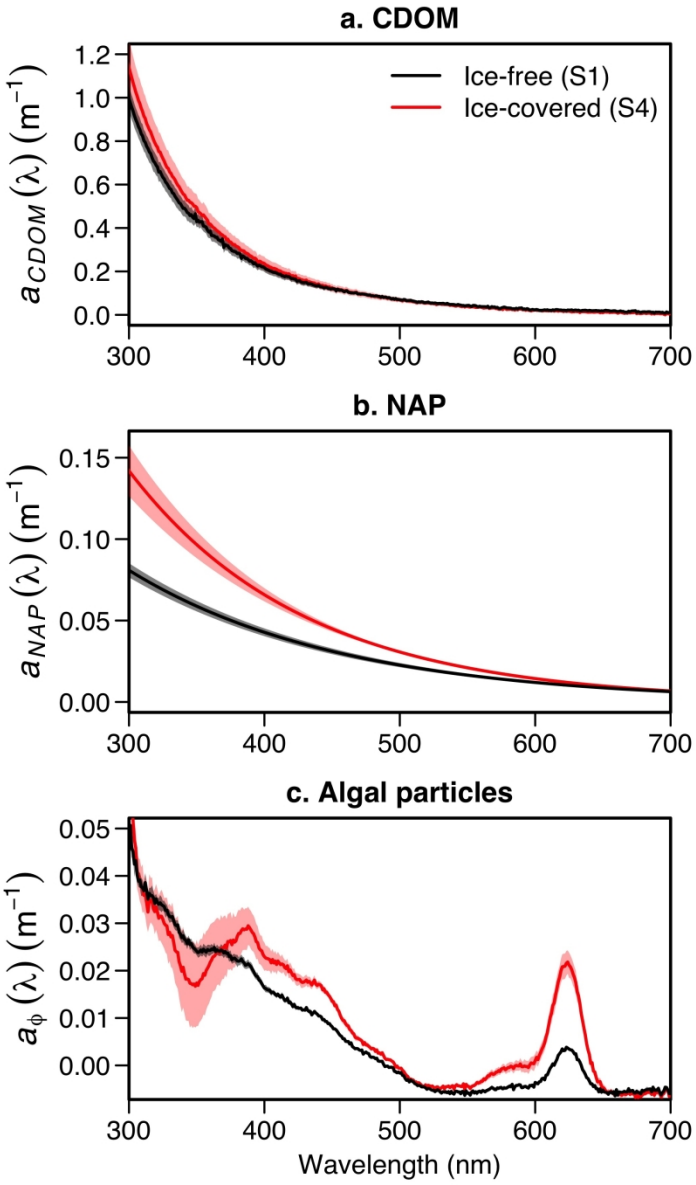

Figure 5. Spectral absorption coefficients for Ward Hunt Lake water samples. The coefficients are for: a) CDOM, $a_{CDOM}(\lambda)$; b) non-algal particles, $a_{NAP}(\lambda)$; and c) algal particles, $a_{\phi}(\lambda)$. The samples were from the upper water column at sites S1 and S4. The shading represents ±SE for triplicate samples.

740x1270mm (72 x 72 DPI)

© The Author(s) or their Institution(s)

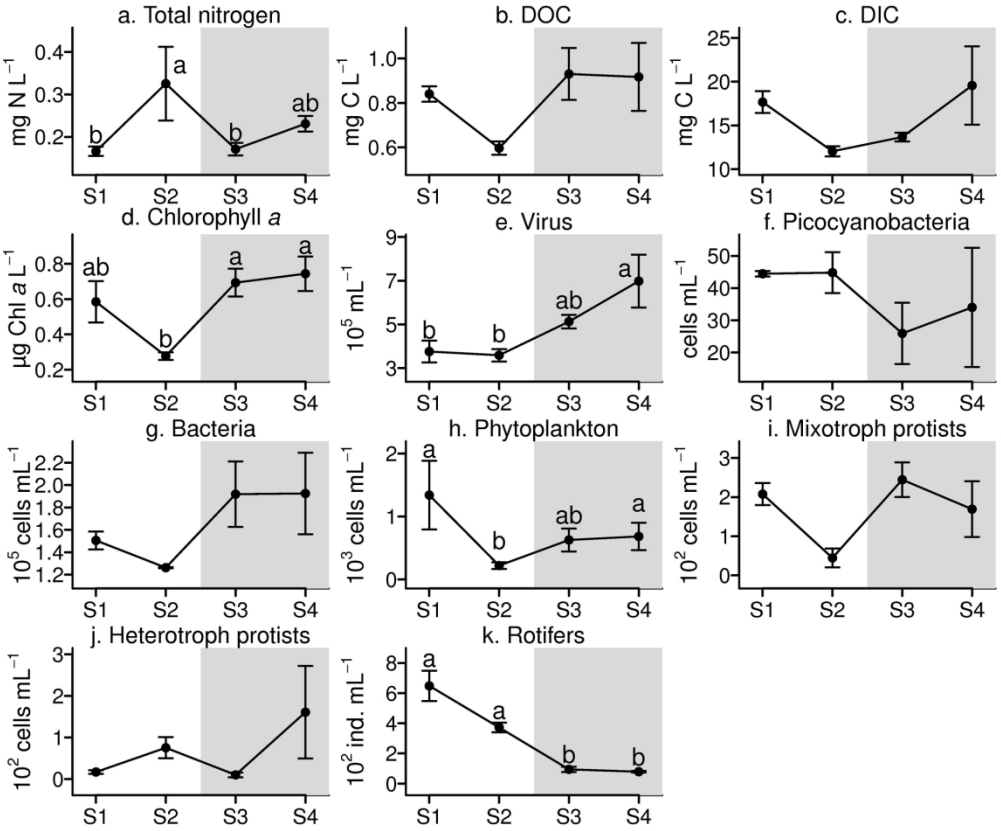

Figure 6. Limnological gradients along the inshore-offshore transect in Ward Hunt Lake, July 2015. Values are means and SE for triplicates; different letters represent significant differences between the sites according to a Tukey HSD multiple comparison following a significant ANOVA. Results of the ANOVA comparisons of sites: a) Total nitrogen: $F_{3,8} = 5.75$, P = 0.047; b) Dissolved organic carbon (DOC): $F_{3,8} = 4.57$, P = 0.060; c) Dissolved inorganic carbon (DIC): $F_{3,8} = 3.26$, P = 0.098; d) Chlorophyll *a*: $F_{3,7} = 6.62$, P = 0.047; e) Viruses: $F_{3,8} = 5.87$; P = 0.047; f) Picocyanobacteria: $F_{3,8} = 1.39$, P = 0.315; g) Bacteria: $F_{3,8} = 5.06$, P = 0.054; h) Phytoplankton: $F_{3,8} = 6.166$, P = 0.047; i) Mixotrophic protists: $F_{3,8} = 3.58$, P = 0.091; j) Heterotrophic protists: $F_{3,8} = 1.97$, P = 0.218; k) Rotifers: $F_{3,8} = 58.28$, P < 0.001.

184x152mm (300 x 300 DPI)

© The Author(s) or their Institution(s)

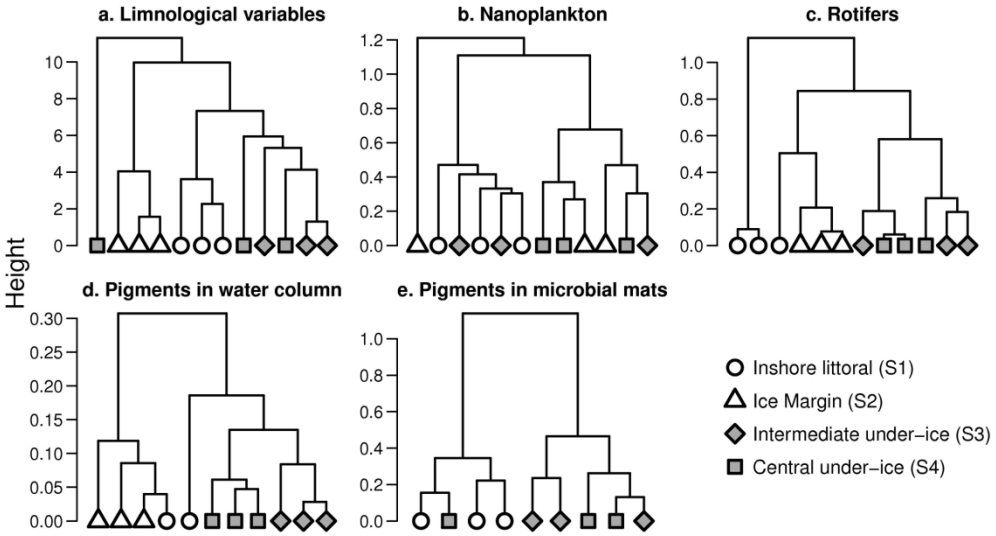

Figure 7. Cluster analysis of limnological variables, biological communities and pigments along the inshore-offshore transect in Ward Hunt Lake, July 2015. Dendrograms represent Ward clustering performed on the following distance matrices: standardized Euclidian distances for limnological variables and Bray-Curtis distances for nanoplankton, rotifers and pigment assemblages. Points filled with gray denote sites covered by ice.

184x101mm (300 x 300 DPI)

© The Author(s) or their Institution(s)

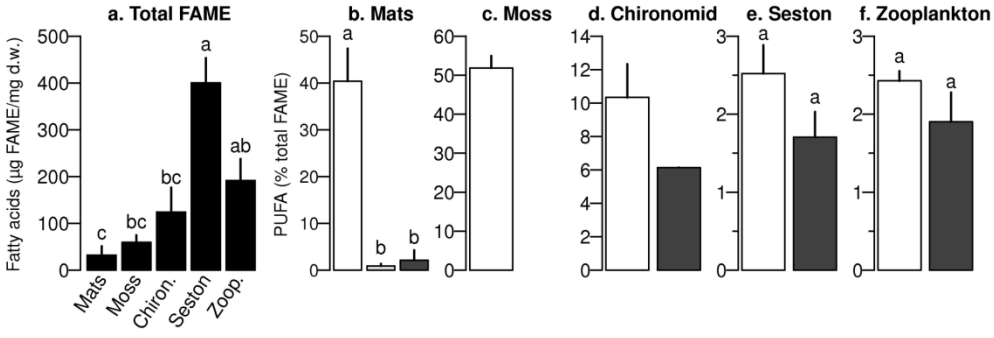

Figure 8. Fatty acid methyl esters (FAME) in samples from Ward Hunt Lake at the inshore moat (S1, in white), intermediate under-ice (S3, in grey) and central under-ice (S4, in black) sites: a) total FAME concentration in µg/mg dry weight; proportion of polyunsaturated fatty acids (PUFA) in b) microbial mats, c) mosses, d) chironomid larvae, e) seston, and f) zooplankton, expressed as percent of total FAME in their respective zones. Values are means for triplicates with SE, except for inshore mats and chironomids (n=2) and central chironomid larvae (n=1). Results of the ANOVA comparisons of total FAME: in food web compartments in panel a) $F_{4,22}$=5.75, P=0.02; in mats in panel b) $F_{2,6}$=16.85, P=0.003; in seston in panel e) $F_{1,5}$=2.77, P=0.16; and in zooplankton in panel f) $F_{1,5}$=2.65, P=0.20. Chironomid larvae were not tested due to insufficient numbers of samples.

184x65mm (300 x 300 DPI)

© The Author(s) or their Institution(s)

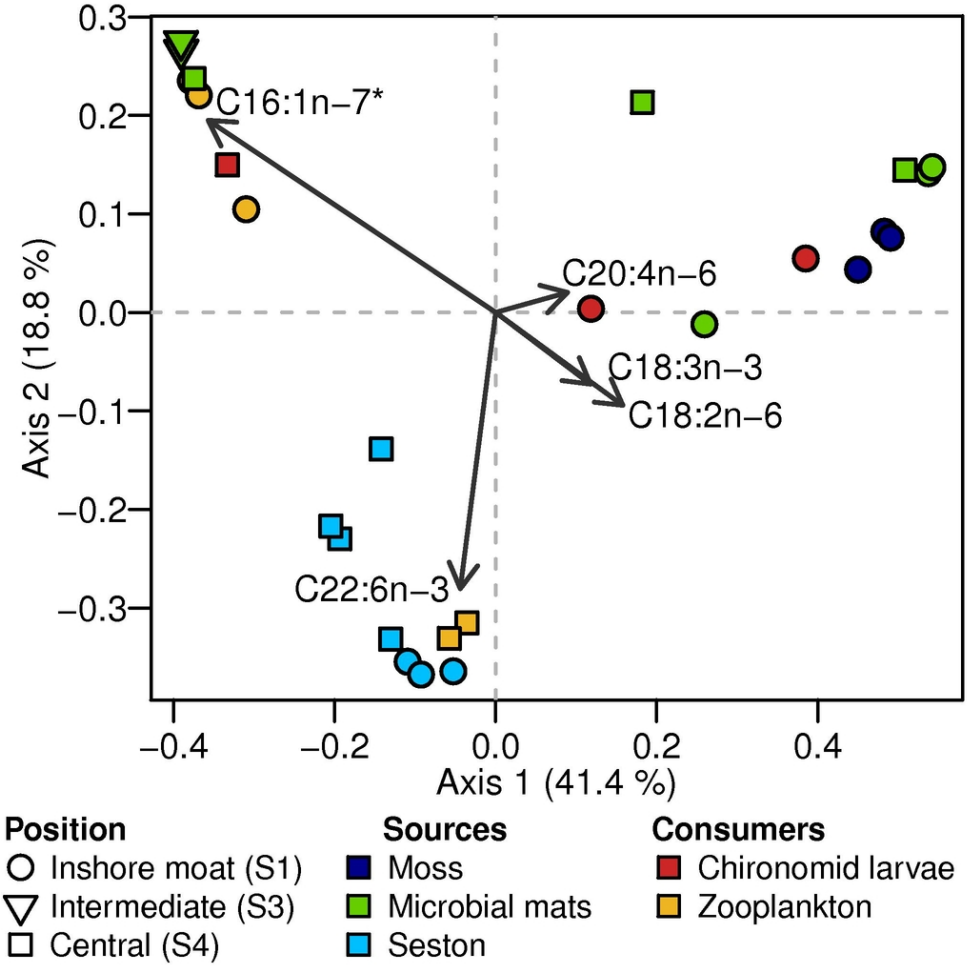

Figure 9. Principal coordinate analysis (PCoA) of fatty acids in the Ward Hunt Lake food web. Samples were from the inshore moat (S1), intermediate under-ice (S3) and central under-ice (S4) sites. Arrows represent the contribution of the five most influential fatty acids for the distribution of samples. *Length of the C16:1n-7 arrow was divided by 3.

88x88mm (300 x 300 DPI)

© The Author(s) or their Institution(s)